

THE LOW-REDSHIFT QUASAR-QUASAR CORRELATION FUNCTION FROM AN EXTRAGALACTIC H α EMISSION-LINE SURVEY TO Z=0.4

C.N. SABBAY^{1,2}, A. OEMLER³, P. COPPI¹, C. BALTAY⁴, A. BONGIOVANNI^{5,6}, G. BRUZUAL⁵, C.E.
GARCIA⁷, J. MUSSER⁸, A.W. RENGSTORF⁸, J.A. SNYDER⁴

Draft version November 2, 2018

ABSTRACT

We study the large-scale spatial distribution of low-redshift quasars and Seyfert 1 galaxies using a sample of 106 luminous emission-line objects ($\overline{M}_B \approx -23$) selected by their H α emission lines in a far-red objective prism survey ($0.2 < z < 0.37$). Of the 106 objects, 25 were previously known AGN (Veron-Cetty and Veron 2000), and follow-up spectroscopy for an additional 53 objects (including all object pairs with separation $r < 20 h^{-1}$ Mpc) confirmed 48 AGN and 5 narrow emission-line galaxies (NELGs). The calculated amplitude of the spatial two-point correlation function for the emission-line sample is $A = 0.4 \cdot \bar{\xi}(r < 20 h^{-1} \text{ Mpc}) \cdot 20^{1.8} = 142 \pm 53$. Eliminating the confirmed NELGs from the sample we obtain the AGN clustering amplitude $A = 98 \pm 54$. Using Monte Carlo simulations we reject the hypothesis that the observed pair counts were drawn from a random distribution at the 99.97% and 98.6% confidence levels for the entire sample and the AGN subset respectively. We measure a decrease in the quasar clustering amplitude by a factor of 3.7 ± 2.0 between $z = 0.26$ and $z \approx 1.5$, and present the coordinates, redshifts, and follow-up spectroscopy for the 15 previously unknown AGN and 4 luminous NELGs that contribute to the clustering signal.

Subject headings: cosmology: large scale structure of universe — galaxies: clusters: general — surveys

1. INTRODUCTION

With the emergence of systematic quasar surveys of relatively high surface density in the early 1980's, the study of the large-scale spatial distribution of quasars became an active area of research (c.f. Osmer 1981). Currently, there are numerous measurements of the mean clustering properties of quasars at $1 \lesssim z \lesssim 2$ (e.g., Croom and Shanks 1996; La Franca, Andreani and Cristiani 1998), with improved constraints expected soon from the 2dF quasar survey (Smith et al. 1996) and the Sloan Digital Sky Survey (Gunn and Weinberg 1995). However, much less work is available at low redshift ($z \lesssim 0.3$), for which the dominant UV-excess technique for selecting quasars is less effective (e.g., Marshall 1985) and relatively small cosmological volumes are sampled. Measurement of the clustering of low-redshift AGN, however, provides the zero point and leverage to discriminate among models for the evolution of large-scale structure.

The primary studies of AGN clustering at low redshift are that of Boyle and Mo (1993) and Georgantopoulos and Shanks (1994). Boyle and Mo measured the correlation function, $\xi(r)$, for an X-ray sample of 183 AGN ($z < 0.2$) selected in the all-sky *Einstein* Extended Medium Sensitivity Survey. At small scales they found a marginal detection

of clustering, $\xi(r < 10 h^{-1} \text{ Mpc}) = 0.7 \pm 0.6$. Georgantopoulos and Shanks investigated the spatial distribution of a far-infrared sample of 192 Seyfert galaxies (56 Sy1 and 136 Sy2) at $z < 0.1$ selected in the all-sky IRAS survey. They detected Seyfert clustering at the $\approx 3\sigma$ confidence level on small scales, with $\xi(r < 20 h^{-1} \text{ Mpc}) = 0.52 \pm 0.13$. By comparison to measurements of quasar clustering at $\bar{z} \approx 1.5$, both groups favored a comoving evolution model, in which $\xi(r)$ is constant with redshift, and marginally excluded a stable evolution model, $\xi(r) \sim (1+z)^{-1.2}$.

We undertake a similar study using a sample of 106 luminous emission-line objects (≈ 95 Sy1/quasar) identified in a large-area objective-prism survey (Sabbey 1999; Sabbey et al. 2000). With the unique far-red bandpass ($6000 < \lambda < 9200\text{\AA}$) of the observations, we are able to select AGN by their H α emission lines to $z \approx 0.4$ for the first time. In contrast to the samples described above, the sample employed here is optically-selected and emphasizes luminous ($\overline{M}_B \approx -23$) Sy1 and quasars at ($0.2 < z < 0.37$), as opposed to lower luminosity Sy2/Sy1 in the nearby universe. In contrast to searching for blue point sources (UV-excess selection, Sandage 1965), the H α survey is relatively independent of object color and morphology, and has a high selection efficiency ($\gtrsim 90\%$) at

¹Yale University, Astronomy Department, 260 Whitney, New Haven CT 06511

²Institute of Astronomy, University of Cambridge, Madingley Road, Cambridge CB3 0HA, UK

³Carnegie Observatories, 813 Santa Barbara St., Pasadena CA, 91101

⁴Yale University, Physics Department, P. O. Box 208121, New Haven CT 06520-8121

⁵Centro de Investigaciones de Astronomía (CIDA), A. P. 264, Mérida 5101-A, Venezuela

⁶Universidad Central de Venezuela, Departamento de Física, 1042 Caracas, Venezuela

⁷Universidad Complutense de Madrid, Dept. de Astrofísica, 28040 Madrid, Spain

⁸Indiana University, Dept. of Astronomy, 319 Swain West, Bloomington IN, 47405

bright (and faint) apparent magnitudes, with a large dynamic range ($12 < m_B < 20$).

2. THE LOW REDSHIFT QUASAR CATALOG

The objective-prism data were taken during seven nights in January through May 1999 with the QUEST 16-CCD driftscan camera on the 1-m Venezuelan Schmidt telescope (Snyder 1998; Sabbey, Coppi, & Oemler 1998). A fully-automated analysis pipeline extracts 1-D spectra and fits a Gaussian profile to all peaks $> 1\sigma$ above the apparent continuum to measure emission-line signal-to-noise ratio (SNR), equivalent width (EW), and center. The minimum SNR required for selection is a function of EW, ranging from SNR > 5.5 for EW $> 50\text{\AA}$ to SNR > 2.5 for EW $> 100\text{\AA}$ (see Sabbey 1999). The survey covers approximately 700 deg^2 in the equatorial region and contains 719 emission-line candidates, of which 11% are previously known emission-line objects and $< 10\%$ are expected to be false detections. The magnitude range is $9.7 \leq m_B \leq 20.2$ (see Fig. 1). Follow-up spectroscopy for a total of 258 emission-line objects (including 88 below the survey detection thresholds) confirmed 97 Sy1 and low- z quasars ($z \leq 0.37$), 25 Sy2 ($z \leq 0.49$), 4 quasars ($1.5 \leq z \leq 2.8$) and 132 NELGs.

Of the 258 follow-up spectra, 135 were obtained using the WIYN Hydra multi-fiber spectrograph (Barden and Armandroff 1995). During April, May, and June 1999 a total of 25 Hydra fields were observed (20 deg^2) to characterize the emission-line sample and establish target selection criteria. Fibers were placed on all objects with a peak above the apparent continuum with SNR $\gtrsim 1.5$. Of the 71 emission-line candidates in the Hydra sample with SNR > 2.5 and EW $> 50\text{\AA}$, 67 were confirmed as actual emission-line objects (three of the four spurious detections were the result of spectrum overlaps in the objective prism data). The remaining 123 follow-up spectra were obtained with a slit spectrograph on the du Pont 2.5m at Las Campanas (during April 1999 and April 2000) and with FLAIR at the AAO (during May 2000). The Las Campanas targets (92 spectra) were preferentially taken from the AGN candidate list (specified below), while the FLAIR targets (31 spectra not including duplicate objects or unclassifiable spectra) were drawn from the full candidate list described above.

The follow-up spectroscopy demonstrated a straightforward selection criterion for identifying AGN in the sample: of the 78 objects in the follow-up sample with a candidate emission-line at $\lambda > 7850\text{\AA}$ (i.e., $z > 0.2$), 60 were Sy1/quasars, 6 were Sy2, and 12 were luminous NELGs. (We identify Sy1/quasars by their broad Balmer lines, FWHM $> 1000\text{ km s}^{-1}$, and Sy2 by the line ratio $\lambda 5007/\text{H}\beta > 10$, or $\lambda 5007/\text{H}\beta > 2.5$ and $0.5 < \lambda 6584/\text{H}\alpha < 1.5$ (Veilleux and Osterbrock 1987). The remaining objects are labelled as NELGs.) In addition, all 116 detections at $\lambda > 7500\text{\AA}$ in the follow-up sample were H α , resulting in extremely reliable H α identification. The relative absence of star-forming galaxies at $z > 0.2$ in our survey is expected due to their faint apparent magnitudes and inverse correlation between luminosity and emission-line EW (e.g., Fig. 4 in Salzer, MacAlpine, and Boroson 1989). In addition, the strong CIV emission of a high redshift quasar is unlikely to be mistaken for H α due to the

expected appearance of Ly α in our bandpass.

Restricting the emission-line candidates to the detections at $\lambda > 7850\text{\AA}$ ($z > 0.2$), with a conservative minimum line SNR > 2.7 (EW $> 100\text{\AA}$), yields a sample of 108 AGN candidates. Based on Veron-Cetty and Veron (2000) and the NASA Extragalactic Database (NED), 25 of the 108 candidates are previously known objects (21 quasars, 3 Sy1, and 1 Sy2). The follow-up spectroscopy described above provided spectra for an additional 55 objects in the AGN candidate list, identifying 45 Sy1/quasar, 3 Sy2, 5 NELGs, and 2 false detections. The two false detections were due to spectrum overlaps (reducing the AGN candidate list to 106 objects), but these had been flagged as possible overlaps based on the proximity of objects of comparable brightness, and no further false detections due to overlaps are expected.

The primary selection effect in the objective prism data is the dependence of the magnitude limit on the emission line equivalent width (e.g., Gratton and Osmer 1987). Of the 10 AGN listed in NED in our $\approx 700\text{ deg}^2$ survey region with $0.2 < z < 0.37$ and USNO $m_B < 17.0$, we independently rediscovered 9 in our AGN candidate list. For $m_B < 18.0$, the fraction rediscovered decreases to 15 out of 25. All but one of these not rediscovered in our AGN candidate list have $z \geq 0.3$, corresponding to the decline in detector quantum efficiency at $\lambda \gtrsim 8500\text{\AA}$. (If we consider the redshift interval $0.0 < z < 0.37$ then the rediscovery rates in our survey increase to 15 out of 16 for USNO $m_B < 17.0$, and 24 out of 36 for USNO $m_B < 18.0$.) Calculations of the expected emission-line SNRs for reasonable H α equivalent width distributions gave results comparable to the rediscovery rates (Sabbey 1999).

A cone diagram of the resulting emission-line catalog of 106 objects (78 confirmed) is shown in Fig. 2, and the sky coordinates are shown in Fig. 3. The objective prism redshift uncertainty is $\sigma_z \approx 0.0042$ (the standard deviation between the prism redshifts and the 53 follow-up redshifts measured using the [OIII] $\lambda 5007$ line), corresponding to a comoving scale of $\approx 9\text{ h}^{-1}\text{ Mpc}$ at the average redshift of the sample $\bar{z} = 0.26$. The survey volume is roughly a section of a torus with a radial extent of $\approx 350\text{ h}^{-1}\text{ Mpc}$ ($\Omega = 1$), a right ascension extent of $> 1000\text{ h}^{-1}\text{ Mpc}$, and a declination extent (thickness) of $\approx 70\text{ h}^{-1}\text{ Mpc}$. There are 19 pairs of objects with separation $r < 20\text{ h}^{-1}\text{ Mpc}$, including one quintuplet and one triplet of objects. Follow-up spectroscopy confirming all objects in pairs except one is shown in Fig. 6, and object coordinates and redshifts are listed in Table 1. A paper in preparation (Sabbey et al. 2000) describes the survey technique further, providing all follow-up spectroscopy, coordinates, redshifts, and spectral line measurements.

3. THE CORRELATION FUNCTION

To quantify the large-scale spatial clustering of the quasar sample, we measure the two-point quasar-quasar correlation function (Peebles 1980):

$$\xi(r) = \frac{N_{\text{obs}}(r)}{N_{\text{rand}}(r)} - 1, \quad (1)$$

where $N_{\text{obs}}(r)$ is the observed number of quasar pairs with comoving separation r , and $N_{\text{rand}}(r)$ is the average number of quasar pairs at that separation scale in random com-

parison catalogs of the same size. The comparison catalogs are generated using both coordinate shuffling and random sampling of the smoothed redshift distribution (Osmer 1981; Iovino & Shaver 1988), yielding similar results (within $0.2\Delta\xi$). We calculate the comoving separations between the quasars within the standard Friedmann model assuming $H_0 = 100 h^{-1} \text{ km s}^{-1} \text{ Mpc}^{-1}$ and $\Omega = 1$ (see Kundic 1997). Qualitatively similar results are obtained in a nearly empty universe, as expected due to the independence of *relative* object separations on Ω_0 (Alcock and Paczyński 1979).

The resulting correlation function is shown in Fig. 4 for the full sample and with the confirmed NELGs removed from the sample. On small scales we detect a marginally significant positive signal (at the 2.7σ and 1.8σ levels). At a scale of $r \sim 30 h^{-1} \text{ Mpc}$, $\xi(r)$ drops below the power law ($\approx 2\sigma$ below), possibly corresponding to a known feature of galaxy auto-correlation functions (see Peebles 1993, pg. 362 and references therein). At larger scales, $\xi(r)$ is consistent with zero within the uncertainties. To quantify the significance of the observed clustering, we use Monte Carlo simulations to test the null hypothesis that the 19 pairs (12 pairs with the NELGs removed) were drawn from an unclustered population. In 10^6 random catalog simulations produced by shuffling the object redshifts, only 254 simulations for the full sample and 13526 simulations for the AGN subset produced as many or more pairs at $r < 20 h^{-1} \text{ Mpc}$. Thus, we reject the hypothesis that the samples do not exhibit clustering on the $r < 20 h^{-1} \text{ Mpc}$ scale at the 99.97% and 98.6% confidence levels.

To compare the measured AGN clustering strength to that of galaxy systems in the local universe and high-redshift quasars (see the following section), we calculate the AGN clustering amplitude A . The volume-averaged two-point correlation function on scales $r < R_0$ is:

$$\bar{\xi}(R_0) = \frac{1}{V} \int_V \xi(r) dV = \frac{3}{R_0^3} \int_0^{R_0} \xi(r) r^2 dr.$$

Substituting in $\xi(r) = Ar^{-1.8}$ we obtain: $A = 0.4\bar{\xi}(R_0)R_0^{1.8}$. When edge effects are negligible, $\bar{\xi}(R_0)$ can be measured by:

$$\bar{\xi}(R_0) = \frac{N_{\text{obs}}(r < R_0)}{N_{\text{rand}}(r < R_0)} - 1,$$

where $N_{\text{obs}}(r < R_0)$ and $N_{\text{rand}}(r < R_0)$ are the number of observed and randomly simulated pairs, respectively, with comoving separations $r < R_0$. We set $R_0 = 20 h^{-1} \text{ Mpc}$, corresponding to our 2σ redshift errors, and obtain $A = 98 \pm 54$ ($N_{\text{obs}} = 12$, $N_{\text{rand}} = 5.67$). Using only objective prism redshifts (i.e., not using any of the available follow-up redshifts) we obtain $A = 113 \pm 56$ ($N_{\text{obs}} = 13$, $N_{\text{rand}} = 5.70$). Removing the one object in Table 1 that has not been confirmed with follow-up spectroscopy (and could be a NELG), we obtain $A = 85 \pm 52$ ($N_{\text{obs}} = 11$, $N_{\text{rand}} = 5.60$).

4. EVOLUTION

We consider three commonly used, although quite simple, “models” for parameterizing clustering evolution with redshift: 1) comoving evolution, $\xi(r) = \text{constant}$, 2) stable evolution, $\xi(r) \sim (1+z)^{-1.2}$, and 3) collapsing evolution,

$\xi(r) \sim (1+z)^{-3}$. Thus, we are assuming evolution of the form:

$$\xi_i(r, z) = A_i(z)r^{-1.8}$$

for a galaxy system i . The dependence of the correlation amplitude on redshift is given by $A_i(z) = A_i^0(1+z)^{-(1.2+\epsilon)}$, where A_i^0 is the clustering amplitude for galaxy system i at $z = 0$, and $\epsilon = -1.2, 0$, and 1.8 in the comoving, stable, and collapsing models. We use measured values of the correlation amplitudes for galaxies, groups, and rich clusters: $A_{\text{Galaxy}}^0 = 21$ (Peebles 1993), $A_{\text{Group}}^0 = 100$ (Bahcall and Choksi 1991), and $A_{\text{Cluster}}^0 = 360$ (Bahcall and Soneira 1983). Although significantly weaker correlation amplitudes for rich clusters have been presented in the literature (e.g., Dalton et al. 1992), it has been suggested that the discrepancy is due to systematic differences in cluster richness (Bahcall and West 1992). We therefore use the larger Bahcall and Soneira (1983) measurement to represent the full range of clustering strengths observed locally.

The measured AGN amplitude is comparable to the amplitude expected for clustering of groups of galaxies, but less consistent with the clustering properties of normal galaxies and rich clusters. We quantify this in terms of the observed number of quasar–quasar pairs with $r < 20 h^{-1} \text{ Mpc}$, and the expected number of pairs for each clustering strength A_i in combination with each evolution model. We first evaluate the $\xi_i(r, z)$ at the average redshift of the observed quasar sample ($z = 0.26$) for the three evolution models, obtaining $\xi_i(r, 0.26)$. Then we integrate $\xi_i(r, 0.26)$ from $r = 0$ to $20 h^{-1} \text{ Mpc}$, obtaining $\bar{\xi}_i(20, 0.26)$. Finally, we multiply $\bar{\xi}_i(20, 0.26)$ by $N_{\text{rand}}(r < 20)$ to obtain the predicted number of quasar–quasar pairs in our sample for each galaxy system clustering strength. That is, $N_{\text{predict}}^i(r < 20) = (1 + \bar{\xi}_i(20, 0.26))N_{\text{rand}}(r < 20)$. The results are shown in Table 2.

The number of observed quasar–quasar pairs is consistent with that predicted for the group clustering strength in each evolution model, but marginally inconsistent (at the 2σ level) with galaxy clustering and our assumed cluster–cluster amplitude. If confirmed with a larger sample, this would suggest that $z \sim 0.3$ quasars tend to be located in small groups of galaxies (groups of 11 ± 8 galaxies based on the current measurement and Eq. 2a in Bahcall and Choksi 1991). Indeed, several imaging studies have indicated that $z \lesssim 0.4$ quasars tend to reside in small to moderate groups of galaxies (see Hartwick and Schade 1990 and references therein). Other studies, however, have suggested that low-redshift quasars inhabit environments similar to normal galaxies (Smith, Boyle, and Maddox 1995).

In Fig. 5 we compare the measured quasar clustering amplitude to measurements at other redshifts. Currently, it is not even clear whether the quasar clustering amplitude decreases with redshift (negative evolution), increases with redshift, or remains constant. Although a number of previous studies reported negative evolution (e.g., Iovino and Shaver 1988; Kruszewski 1988; Iovino, Shaver, and Cristiani 1991), there have also been reports of constant clustering (e.g., Andreani and Cristiani 1992) and positive evolution (e.g., La Franca, Andreani, and Cristiani 1998). Given the large uncertainties, the current measurement at $\bar{z} = 0.26$ is consistent with the assumed quasar clustering

amplitude of $A = 27$ at $\bar{z} \approx 1.4$ (La Franca, Andreani, and Cristiani 1998).

Georgantopoulos and Shanks (GS) measured somewhat weaker clustering in their low- z Sy1 sample ($A = -9 \pm 24$), although this possible discrepancy is only at the 2.0σ level. Such a discrepancy could possibly result from the significantly different samples employed (their non-optical sample contains lower luminosity, relatively nearby AGN). For example, IRAS galaxies are known to be relatively biased against high density regions, and related effects could be manifest in the IRAS Seyfert sample used by GS. Also, possible biases in the environments of low-redshift AGN as a function of AGN luminosity have been suggested (Fisher et al. 1996), and different host galaxies as a function of AGN luminosity or redshift would be relevant because

early-type galaxies are known to cluster more strongly by a factor of several than late-type (Davis and Geller 1976; Loveday et al. 1995).

This work was supported by the National Science Foundation, the Department of Energy, and the National Aeronautics and Space Administration. The Observatorio Astronómico Nacional is operated by CIDA for the Consejo Nacional de Investigaciones Científicas y Tecnológicas. This research has made use of the NASA/IPAC Extragalactic Database (NED) which is operated by the Jet Propulsion Laboratory, California Institute of Technology, under contract with the National Aeronautics and Space Administration. This research also used the VizieR Catalogue Service (Ochsenbein et al. 2000).

REFERENCES

- Alcock, C. & Paczyński, B., 1979, *Nature*, 281, 358
 Andreani, P., and Cristiani, S. 1992, *ApJ*, 398, L13
 Bagla, J.S. 1998, *MNRAS*, 297, 251
 Bahcall, N.A., and Chokshi, A. 1991, *ApJL*, 380, L9
 Bahcall, N.A., and Soneira, R.M. 1983, *ApJ*, 270, 20
 Bahcall, N.A., and West, M.J. 1992, *ApJ*, 392, 419
 Barden, S.C., and Armandroff, T. 1995, *Proc. SPIE*, 2476, 56
 Boyle, B.J., and Mo, H.J. 1993, *MNRAS*, 260, 925
 Croom, S.M., and Shanks, T. 1996, *MNRAS*, 281, 893
 Dalton, G.B., Efstathiou, G., Maddox, S.J., and Sutherland, W.J. 1992, *ApJ*, 390, L1
 Davis, M., Geller, M.J. 1976, *ApJ*, 208, 13
 Loveday, J., Maddox, S.J., Efstathiou, G., Peterson, B.A. 1995, *ApJ*, 442, 457
 Fisher, K.B., Bahcall, J.N., Kirhakos, S., Schneider, D.P. 1996, *ApJ*, 468, 469
 Georgantopoulos, I., and Shanks, T. 1994, *MNRAS*, 271, 773
 Gratton, R.G., & Osmer, P.S. 1987, *PASP*, 99, 899
 Gunn, J.E. & Weinberg D.H. 1995, in *Wide Field Spectroscopy and the Distant Universe* ed. S. Maddox & Aragón-Salamanca (World Scientific, Singapore), 3
 Hartwick, F.D.A., and Schade, D. 1990, *ARA&A*, 28, 437
 Hewett, P.C., Foltz, C.B., & Chaffee F.H. 1995, *AJ*, 109, 1498
 Iovino, A., and Shaver, P.A. 1988, *ApJ*, 330, L13
 Iovino, A., Shaver, P.A., and Cristiani, S. 1991, *ASP Conf. Ser.* 21, ed. D. Crampton (San Francisco: ASP), 202
 Kruszewski, A. 1988, *Acta Astronomica*, 38, 155
 Kundic, T. 1997, *ApJ*, 482, 631
 La Franca, F., Andreani, P., and Cristiani, S. 1998, *ApJ*, 497, 529
 Marshall, H.L. 1985, *ApJ*, 299, 109
 Monet, D., et al. 1996, USNO-SA2.0, (U.S. Naval Observatory, Washington DC)
 Ochsenbein F., Bauer P., & Marcout J., 2000, *A&AS* 143, 221
 Osmer, P.S. 1981, *ApJ*, 274, 762
 Peebles, P.J.E. 1980, *The Large-Scale Structure of the Universe* (Princeton: Princeton Univ. Press)
 Peebles, P.J.E. 1993, *Principles of Physical Cosmology* (Princeton: Princeton Univ. Press)
 Sabbey, C.N. 1999, PhD Thesis, Yale University, <ftp://www.astro.yale.edu/pub/sabbey/thesis.ps.gz>
 Sabbey, C.N., Paolo, C., and Oemler, A. 1998, *PASP*, 110, 1067
 Sabbey, C.N. et al. 2000, *ApJS*, in preparation
 Salzer, J.J., MacAlpine, G.M., and Boroson, T.A. 1989, *ApJS*, 70, 479
 Sandage, A. 1965, *ApJ*, 141, 1560
 Shanks, T., Boyle, B.J., and Peterson, B.A. 1988, *ASP Conf. Ser.* 2, ed. P. Osmer and Phillips M.M. (San Francisco: ASP), 244
 Smith, R.J. et al. 1996, in *New Horizons from Multi-Wavelength Sky Surveys*, IAU Symposium 179
 Smith, R.J., Boyle, B.J., and Maddox, S.J. 1995, *MNRAS*, 277, 270
 Snyder, J. A. 1998, *Proc. SPIE*, 3355, 635
 Surdej J., Swings J.-P., Arp H., & Barbier R. 1982, *A&A* 114, 182
 Veilleux, S., and Osterbrock D.E. 1987, *ApJS*, 63, 295
 Veron-Cetty M.P., Veron P., 2000, *ESO Scientific Report* 19, 1
 Voges et al. 1999, *A&A*, 349, 389
 White, R.L., Becker, R.H., Helfand, D.J., & Gregg, M.D. 1997, *ApJ*, 475, 479

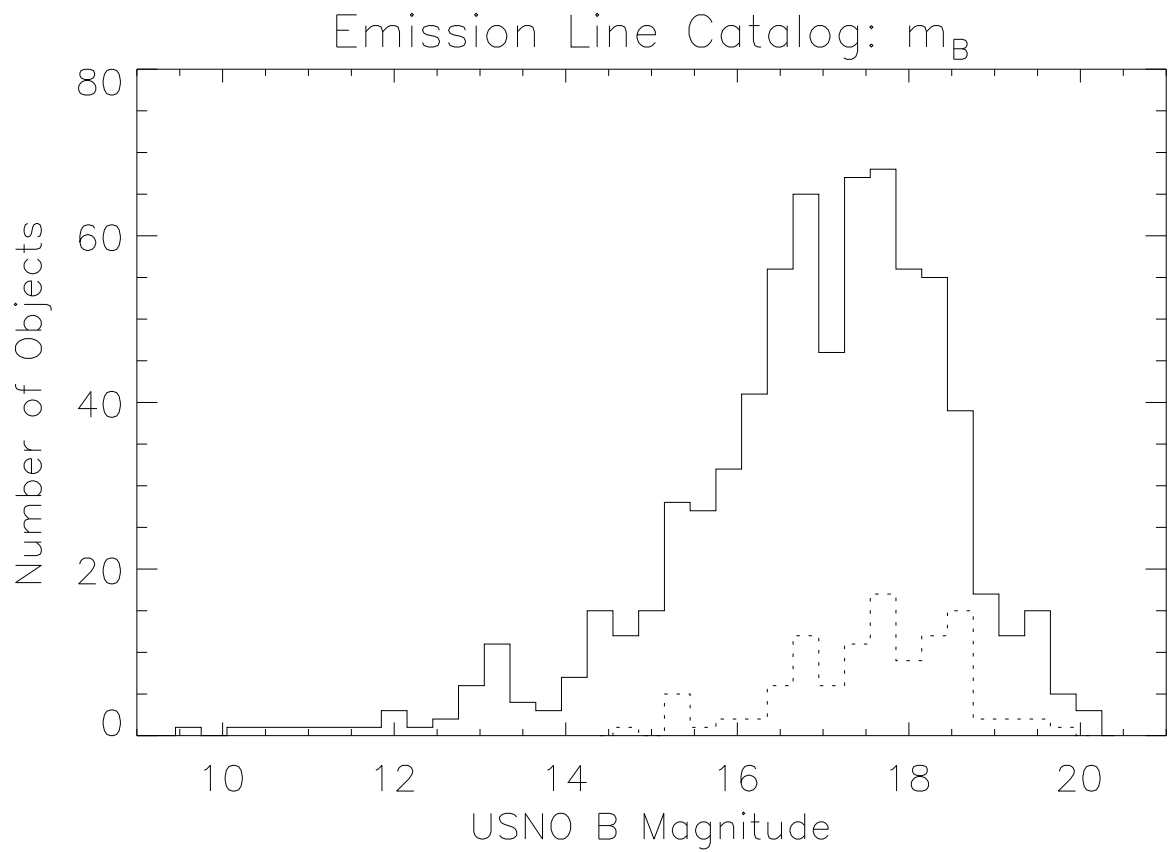


FIG. 1.— The histogram of USNO B magnitudes (Monet et al. 1999) is shown for the entire emission-line catalog of 719 objects, and the ($0.2 < z < 0.37$) subset of 106 AGN candidates used in this paper (dashed lines).

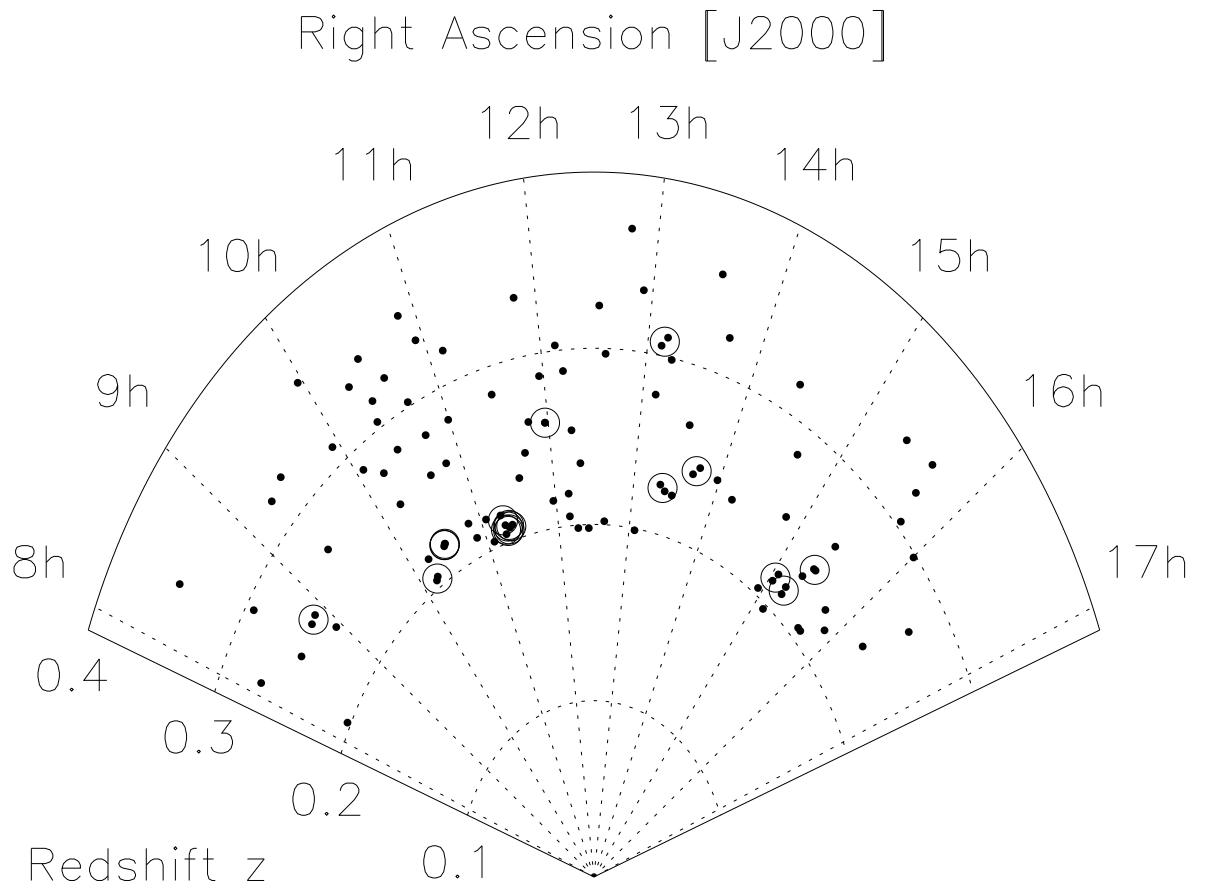


FIG. 2.— A cone diagram of the emission-line sample of 106 objects is shown. The 19 pairs with comoving separation $r < 20 h^{-1}$ Mpc are circled.

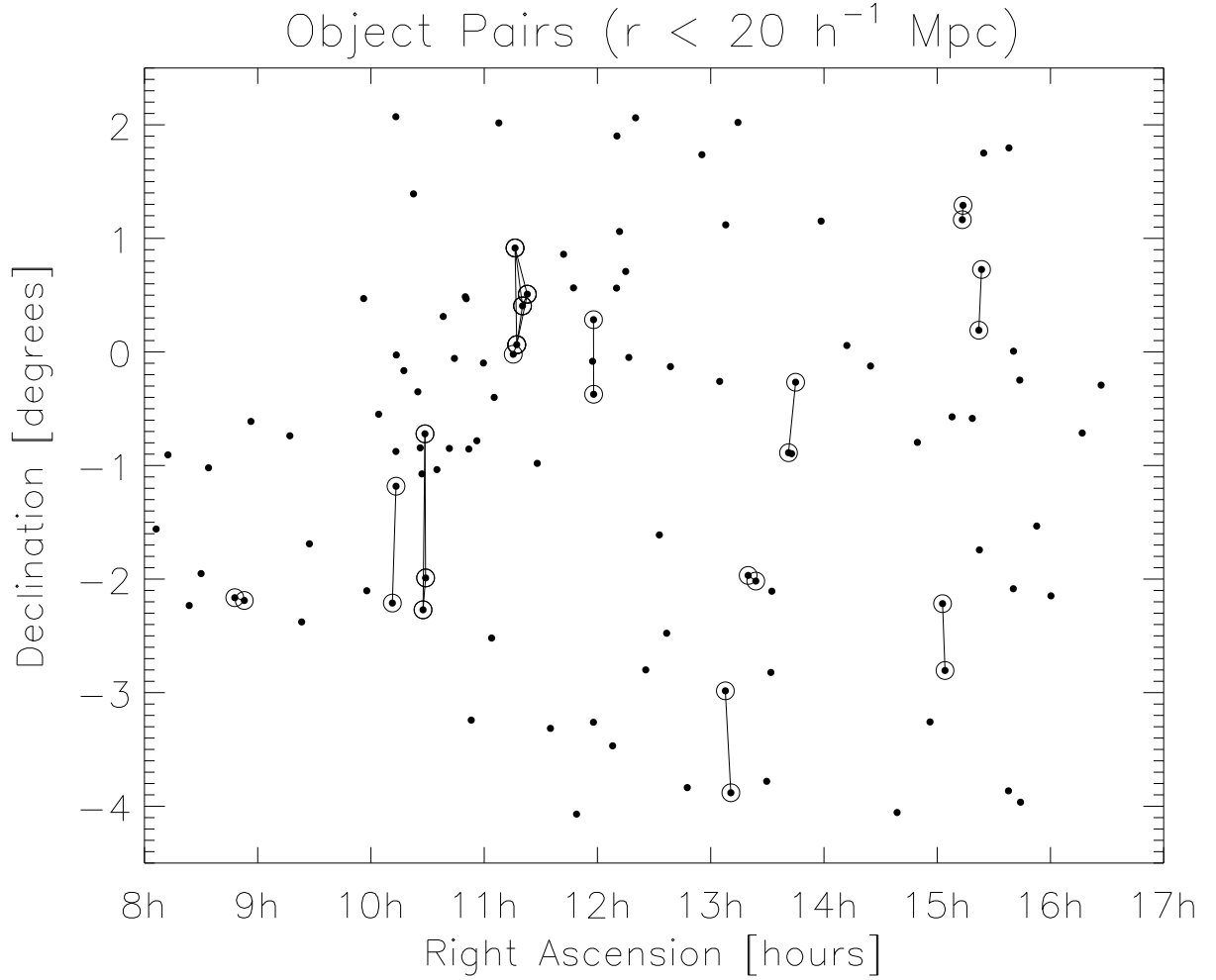


FIG. 3.— The sky coordinates of the sample of 106 AGN candidates are shown. The 19 pairs with comoving separation $r < 20 h^{-1} \text{ Mpc}$ are circled. There is a cluster of five objects near 11h 15m (on a size scale of $\approx 30 h^{-1} \text{ Mpc}$) and a triplet near 10h 30m. The survey region ($\approx 700 \text{ deg}^2$) extends from about 9h 45m to 16h 15m in the declination range $-4.3 < \delta < 2.1$, with extensions to 8h and to 17h at $-0.1 < \delta < -2.2$ (the precise boundaries are jagged and a function of exposure time due to the driftscan nature of the observations).

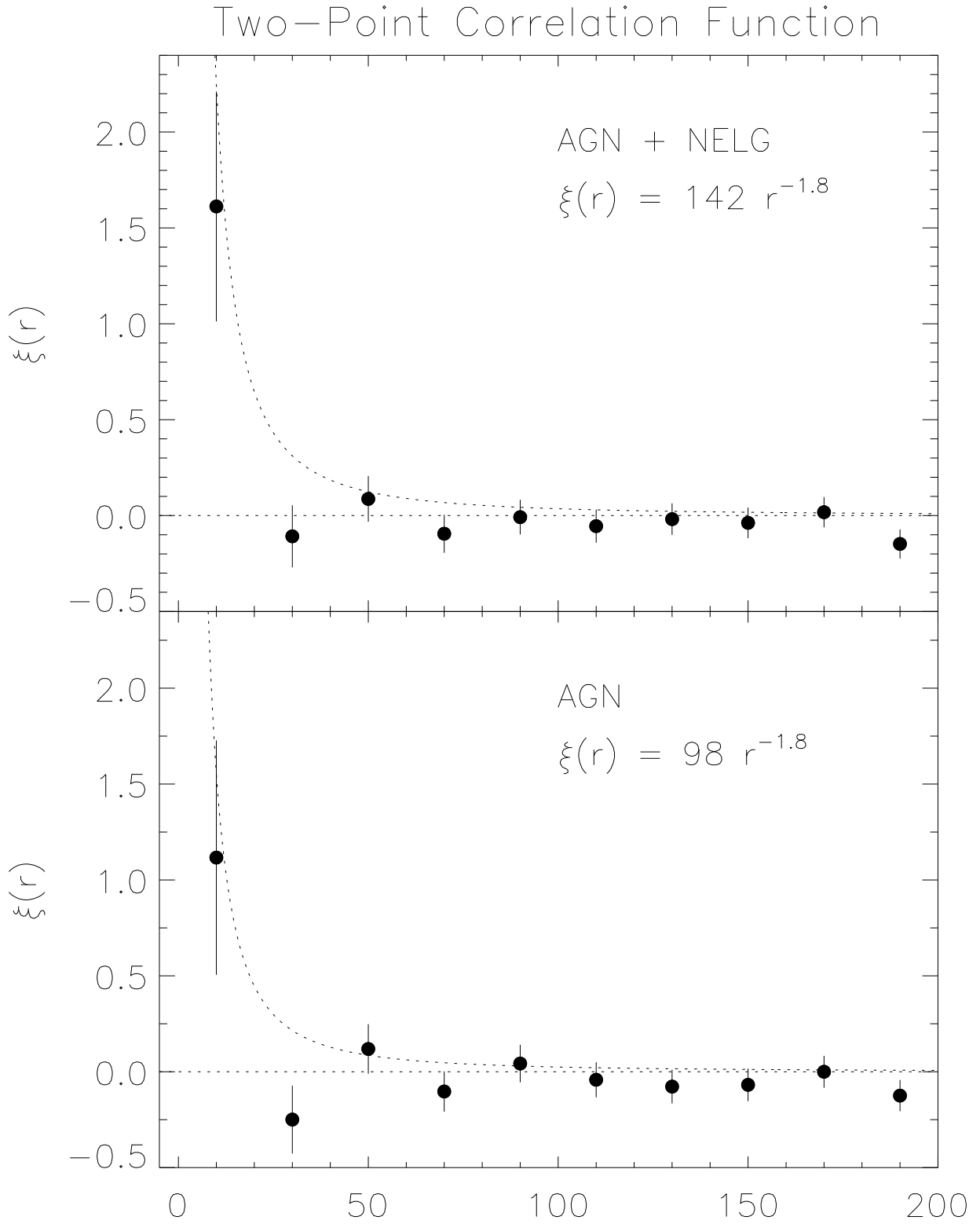


FIG. 4.— The $\bar{z} = 0.26$ correlation function in redshift space with bin sizes of $20 h^{-1}$ Mpc is shown for the emission-line sample (top plot), and the AGN subset (bottom plot). The uncertainties are from the error estimator $\Delta\xi(r) = [(1 + \xi(r))/N_{\text{rand}}]^{0.5}$. The $r^{-1.8}$ power laws with amplitude $A = \xi(1 h^{-1} \text{ Mpc}) = 142$ and 98 as calculated in the text are overlotted.

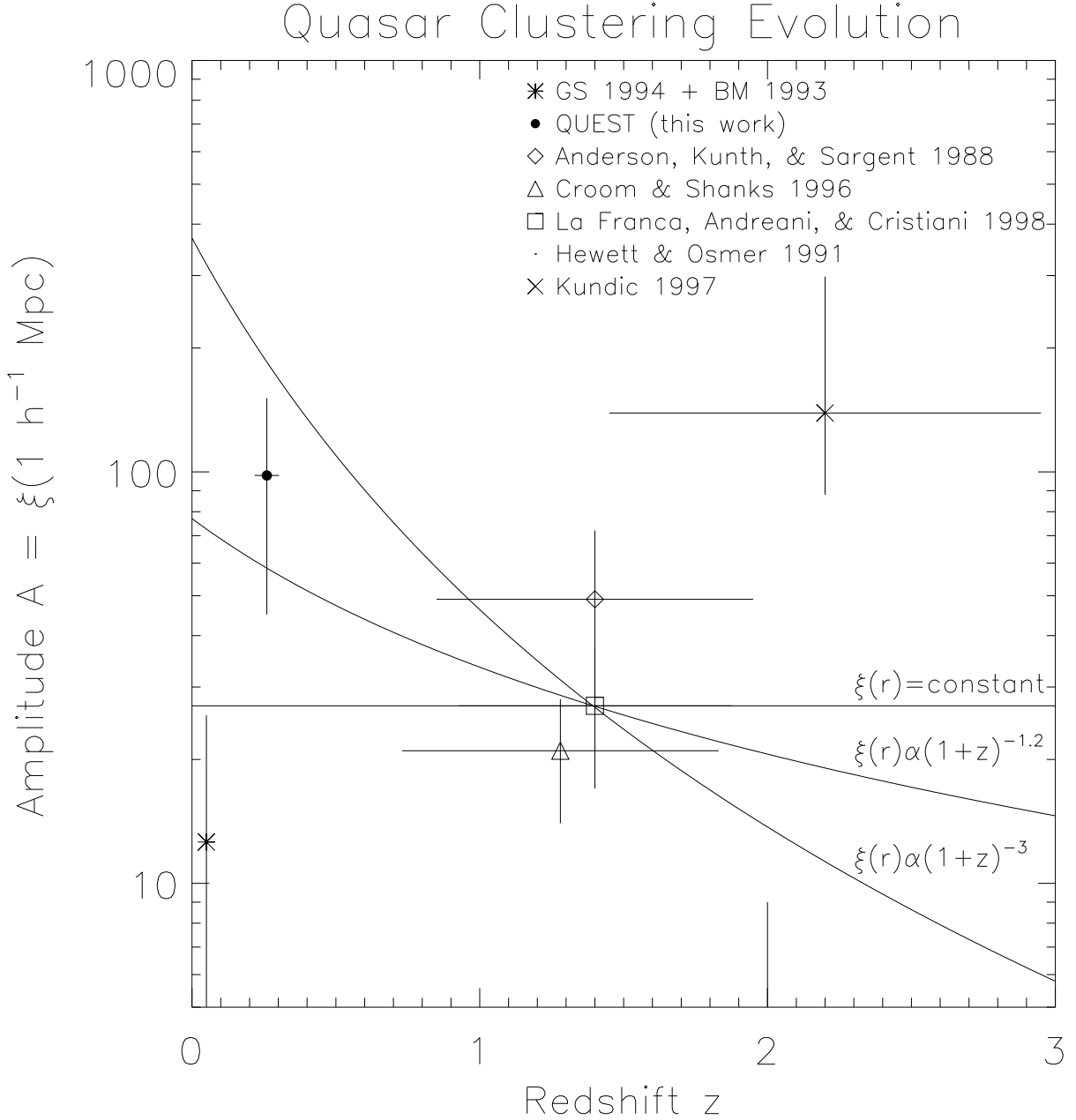


FIG. 5.— The measured quasar-quasar correlation amplitude as a function of redshift based on a representative set of publications. The full width of the horizontal “error bars” indicate 1/2 of the survey redshift extent. The $z = 0.05$ measurement is from the combined Georgantopoulos and Shanks (1994) and Boyle and Mo (1993) samples (see La Franca et al. 1998). For the Sy1 sample of Georgantopoulos and Shanks (1994), the amplitude is $A = -9 \pm 24$ (not shown). The Osmer and Hewett (1991) measurement at $z = 2.0$ is $A = -18 \pm 27$. The $\bar{z} = 0.26$ measurement, combined with the previous low-redshift AGN clustering measurements, is consistent with clustering measurements at $\bar{z} \approx 1.5$ (suggesting weak or no evolution of quasar clustering out to intermediate redshift).

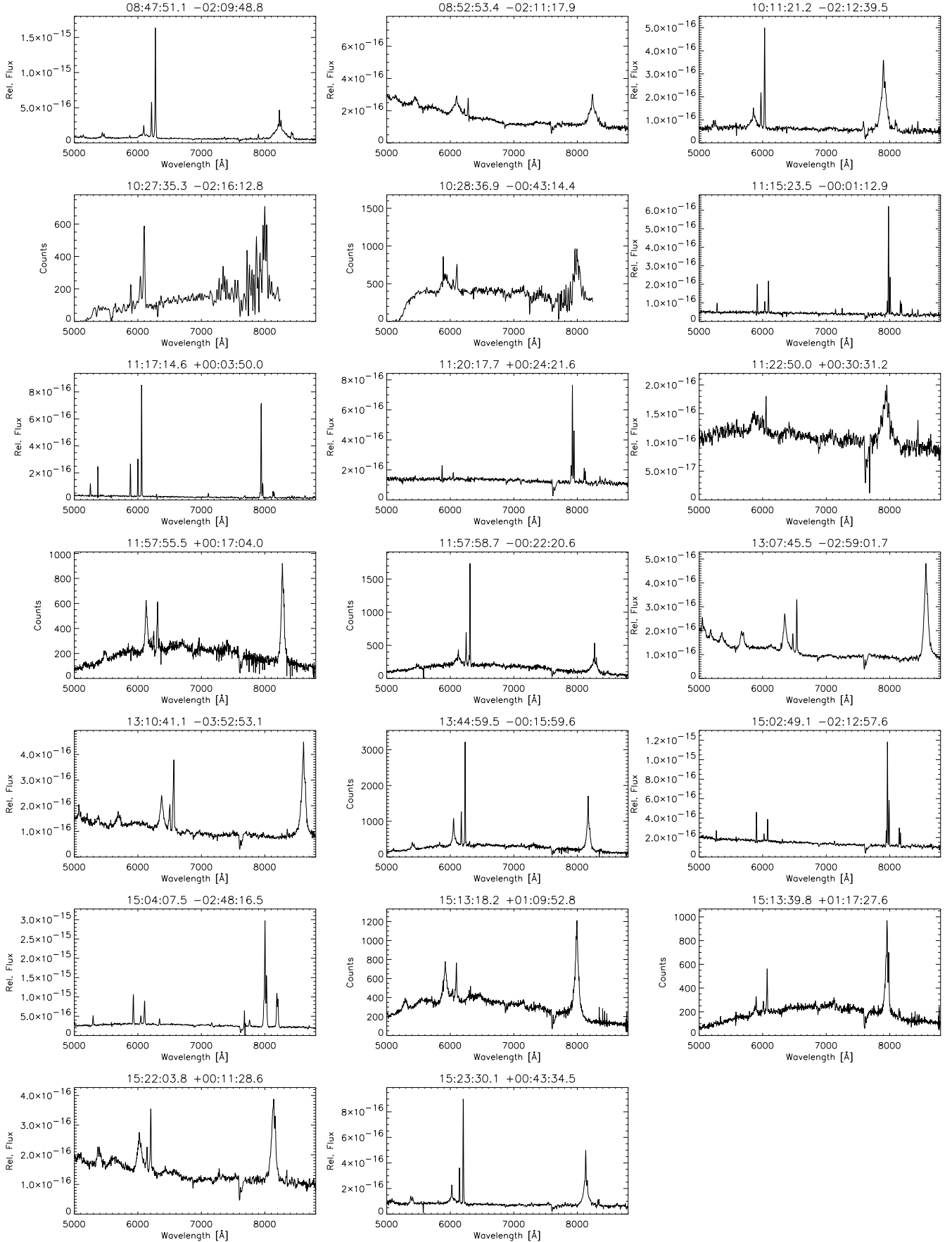


FIG. 6.— The follow-up spectroscopy is shown for the emission-line objects that contribute to the clustering signal on scales $r < 20 h^{-1}$ Mpc (see Table 1).

TABLE 1
 OBJECTS CONTRIBUTING TO CLUSTERING SIGNAL ($r < 20 h^{-1}$ MPC)

Name	R.A. (J2000)	Dec (J2000)	m_B	z	Non-Optical ^{3,4}	Sp Class	Ref
QUEST0847-0209	08:47:51.1	-02:09:48.8	17.8	0.2534	FIRST/RASS	QSO	
QUEST0852-0211	08:52:53.4	-02:11:17.9	16.9	0.2545		QSO	
QUEST1011-0212	10:11:21.2	-02:12:39.5	18.4	0.2045		QSO	
Q1010-0056	10:13:17.2	-01:10:56.1	18.4	0.202	RASS	QSO	1
QUEST1027-0216	10:27:35.3	-02:16:12.8	18.1	0.2180	FIRST	AGN	
QUEST1028-0043	10:28:36.9	-00:43:14.4	17.6	0.2189		QSO	
Q1026-0144	10:28:57.2	-01:59:22.8	16.8	0.217		QSO	1
QUEST1115-0001	11:15:23.5	-00:01:12.9	19.7	0.2165		NELG	
QUEST1116+0054 ^a	11:16:19.9	+00:54:56.6	18.6	0.205			
QUEST1117+0003	11:17:14.6	+00:03:50.0	19.3	0.2101		NELG	
QUEST1120+0024	11:20:17.7	+00:24:21.6	18.6	0.2077	FIRST	NELG	
QUEST1122+0030	11:22:50.0	+00:30:31.2	17.9	0.2088	RASS	QSO	
QUEST1157+0017	11:57:55.5	+00:17:04.0	18.6	0.2603	RASS	QSO	
QUEST1157-0022	11:57:58.7	-00:22:20.6	17.0	0.2603	RASS	QSO	
QUEST1307-0259	13:07:45.5	-02:59:01.7	17.6	0.3056		QSO	
QUEST1310-0352	13:10:41.1	-03:52:53.1	17.2	0.3109	RASS	QSO	
Q1317-0142	13:19:50.4	-01:58:03.5	16.8	0.225	FIRST	QSO	1
Q1321-0145	13:23:52.8	-02:01:01.7	17.5	0.224	FIRST/RASS	QSO	1
UM602	13:41:13.9	-00:53:14.8	17.4	0.237	FIRST/RASS	QSO	2
Q1342-000	13:44:59.5	-00:15:59.6	17.1	0.245	RASS	QSO	2
QUEST1502-0212	15:02:49.1	-02:12:57.6	17.4	0.2139	FIRST	NELG	
QUEST1504-0248	15:04:07.5	-02:48:16.5	16.6	0.2194	FIRST/RASS	QSO	
QUEST1513+0109	15:13:18.2	+01:09:52.8	17.6	0.2174		QSO	
QUEST1513+0117	15:13:39.8	+01:17:27.6	18.4	0.2123		QSO	
QUEST1522+0011	15:22:03.8	+00:11:28.6	17.6	0.2389		QSO	
QUEST1523+0043	15:23:30.1	+00:43:34.5	17.8	0.2391	RASS	QSO	

REFERENCES.— (1) Hewett, Foltz, and Chaffee 1995; (2) Surdej et al. 1982; (3) Voges et al. 1999; (4) White et al. 1997.

^aFor this object only a redshift estimate from objective prism data is available.

TABLE 2
 THE OBSERVED, RANDOM, AND PREDICTED QUASAR-QUASAR PAIR COUNTS WITH SEPARATION $r < 20 h^{-1}$ MPC
 ($\Omega = 1$)

N_{rand}	N_{obs}	$N_{\text{predict}}^{\text{Galaxy}}$	$N_{\text{predict}}^{\text{Group}}$	$N_{\text{predict}}^{\text{Cluster}}$	$N_{\text{predict}}^{\text{QSO}}$	Evolution Model
5.56	12	7.02 -1.9σ	12.12 0.0σ	28.90 $+3.1\sigma$	7.42 -1.7σ	Comoving
5.56	12	6.70 -2.1σ	10.56 -0.4σ	23.27 $+2.3\sigma$	9.44 -0.8σ	Stable
5.56	12	6.35 -2.2σ	8.90 -1.0σ	17.28 $+1.3\sigma$	17.71 $+1.4\sigma$	Collapsing